Beam vibration due movement of overweight cargoes on reinforced concrete bridges at different ground conditions

M. Berdibaev[1*], *B.* Mardonov[1], *N.* Nishonov[1], and *Z.* Rakhimjonov[2]

[1]Academy of Science of the Republic of Uzbekistan Institute of Mechanics and Seismic Stability of Structures named after M.T. Urazbaev, Tashkent, Uzbekistan
[2]Tashkent state Transport university, Tashkent, Uzbekistan

Abstract. The article deals with the vibrations of a reinforced concrete bridge whose supports are located in soils with different properties under the action of overweight cargoes. The assumption is made that the structure deformed in the elastic zone when Hooke's law is valid. The Fourier method is used to solve the problem. The results are presented as graphs of changes in stresses and deflections along the coordinate and time, which are accompanied by analysis. When a concentrated load is applied, depending on the stiffness coefficient of the connection between the supports and the ground, stresses exceeding the limit load can occur in the middle of the beam cross-section. Thus, in the calculations, it is necessary to consider the nature of the interaction of the supports with the surrounding soils when calculating the beams for the action of moving loads.

1 Introduction

The development of transport infrastructure makes it possible to create large integrated cities, thereby opening up new prospects for the socio-economic development of regions. Bridge constructions, as a type of transport infrastructure, are usually aimed primarily at the internal development of a country, improving transport accessibility and enhancing inter-regional connections.

In the world, various transport structures, including bridge structures, are important for expanding trunk road networks, increasing passenger and freight transport, and developing infrastructure in large cities. Bridge structures, as a construction product, have specific consumer properties that determine their purpose and quality [1]. Research on the dynamic response of bridges due to moving loads has received considerable attention with the passing of recent years. Several mathematical models of vehicles were developed with the passing of years [2].

The study and analysis of oscillating processes of transport structures under moving loads are becoming even more important nowadays with changing conditions. This is due to increasing traffic speeds, with the proportion of multi-axle and heavily laden vehicles in

* Corresponding author: mars.berdibaev@mail.ru

the overall traffic flow continuously increasing. On the other hand, every year, more and more transport structures, due to the increased dynamic impact from vehicles and improper use, develop defects and damages that, even when subjected to short-term and even more long-term impacts, change the nature of the vibrations of structures under moving loads and can affect the durability of the structure.

The problem of assessing the dynamic impact of road and railroad loads on bridge spans is important to ensure the reliability of structures both at the design stage of new bridges and during the reconstruction and operation of existing bridges. New structures, where restrictions are generally not imposed, may also receive significant dynamic impacts from the passing load due to the span structure's structural and static design deficiencies. In this connection, creating a scientifically substantiated modern methodology for assessing the dynamic effects of moving loads on road bridge spans is an urgent task [2-5].

The study of the dynamic impact of vehicles is especially important for road bridges with increased deformability. In this situation, the forces of inertia of the vehicle moving on the bridge become significant and begin to affect the overall oscillatory process. A characteristic feature of the operation of the transport structure is unsteady dynamic effects. At the same time, the intensive development of computing technology makes it possible to simulate the dynamic behavior of discrete-continuous and continuum systems whose mathematical model is described by refined partial differential equations. Note also that an increase in the carrying capacity of vehicles leads to the emergence of new qualitative and quantitative features and effects of the dynamic impact, which previously did not manifest themselves or were insignificant. To study the peculiarities of the dynamic impact of moving loads on bridge structures in modern conditions, existing approaches become insufficient, and dynamic calculation methods need to be improved and developed. All this confirms the importance and relevance of solving the problem of changing the dynamic responses of transport structures to moving loads [6-20].

2 Objects and methods of research

Most transport structures for passing a variety of moving loads are complex dynamic oscillating systems with distributed parameters and are, therefore, continuous. To assess the reliability and carrying capacity of such engineering structures under the action of nonstationary dynamic influences, complex, modern, and perfect calculation methods are used. The algorithms developed on their basis are implemented using intensively developing computer technology and application software packages. This allows you to perform a sufficient number of computational experiments to get a complete picture of the structure's deflection. However, in several cases, it is possible to assess the reliability of a structure with sufficient accuracy, reasonably using the simplicity of calculation methods in the classical formulation without involving complex and modern calculation methods. In this case, it is necessary to determine the limits of using one or another simplified variant of the statement of such a problem. On the other hand, each of the options can be improved to generalize the problem and expand its scope.

1. Figure 1 shows a single-span reinforced concrete road bridge. Consider bridge abutments as rigid bodies interacting with the ground, subject to nonstationary dynamic forces. Set the origin at the point O. The Ox axis coincides with the neutral axis of the beams, and the Oy_1 axis with its origin at O_1 is perpendicular to it (Fig. 2).

Fig. 1. Reinforced concrete bridge with road beam

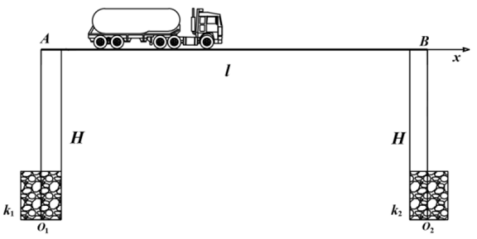

Fig. 2. Calculation diagram of a road single-span beam bridge with moving loads

Consider the case where a moving load acts on the beam in the form of Dirac delta function $P\delta(v_0t-x)$ (v_0 − speed of the moving uniform, P is the magnitude of the acting load per unit length of the beam), where the Ox axis coincides with the beam axis, the origin of the coordinates is located in the right beam support (fig. 3). The deflections of the beam $W(x, t)$ satisfy the equation

$$EJ\frac{\partial^4 W}{\partial x^4}+m_b\frac{\partial^2 W}{\partial t^2}=P\delta(v_0t-x) \tag{1}$$

and the following initial and boundary conditions

$$\frac{\partial W}{\partial x}=0,\ M_1\frac{\partial^2 W}{\partial t^2}=EJ\frac{\partial^3 W}{\partial x^3}-k_1W \quad \text{for } x=0 \tag{2}$$

$$\frac{\partial W}{\partial x}=0,\ M_2\frac{\partial^2 W}{\partial t^2}=-EJ\frac{\partial^3 W}{\partial x^3}-k_2W \quad \text{for } x=l, \tag{3}$$

where m_b is beam linear weight, E is the Young's modulus of the material of the beam, J_z is the moment of inertia of the section, l is the length of the span, M_1 and M_2 are the weights of the left and right supports, k_1 and k_2 are the longitudinal shear coefficients on the contact surface of the supports with soils.

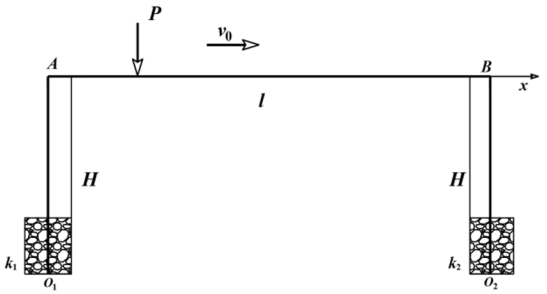

Fig. 3. Calculation scheme of moving concentrated load

Equation (1) is solved by the Fourier method, and the solution of the corresponding homogeneous equation is presented as

$$W=\varphi(x)\cdot T(t)$$

Assuming $T'' = -\omega^2 T$, we get

$$\varphi^{IV} - \bar{\lambda}^4 \varphi = 0, \left(\bar{\lambda}^4 = \frac{m_b \omega^2}{EJ} \right). \quad (4)$$

The solution of equation (4) is presented through the Krylov functions

$$\varphi = C_1 Y_1 + C_2 Y_2 + C_3 Y_3 + C_4 Y_4, \; Y_1(x) = (chx + \cos x)/2,$$
$$Y_2(x) = (shx + \sin x)/2, \; Y_3(x) = (chx - \cos x)/2, \quad Y_4(x) = (shx - \sin x)/2,$$

where the constants C_i (i=1, 2, 3, 4), according to conditions (2) and (3), satisfy equations

$$\begin{aligned} C_2 &= 0, \\ \gamma_1(\lambda) C_1 - \lambda^3 C_4 &= 0, \\ C_1 Y_4(\lambda) + C_3 Y_2(\lambda) + C_4 Y_3(\lambda) &= 0, \\ C_1 R_4(\lambda) + C_3 R_2(\lambda) + C_4 R_3(\lambda) &= 0, \end{aligned} \quad (5)$$

where $R_4 = \gamma_2(\lambda) Y_1(\lambda) + \lambda^3 Y_2(\lambda)$, $R_2 = \gamma_2(\lambda) Y_3(\lambda) + \lambda^3 Y_4(\lambda)$, $R_3 = \gamma_2(\lambda) Y_4(\lambda) + \lambda^3 Y_1(\lambda)$, $\gamma_i = \beta_i - \alpha_i \lambda^4$, $\lambda = \bar{\lambda} l$, $\beta_i = k_i l^3 / EJ$, $\alpha_i = m_0 l / m_i$.

After excluding the constant C_4, the last equations are reduced to the form

$$\begin{aligned} C_1 F_{11}(\lambda) + C_3 F_{12}(\lambda) &= 0, \\ C_1 F_{21}(\lambda) + C_3 F_{22}(\lambda) &= 0, \end{aligned}$$

where $F_{11} = \gamma_1 Y_3(\lambda) + \lambda^3 Y_4(\lambda)$, $F_{12} = \lambda^3 Y_2(\lambda)$ $F_{21} = \gamma_1 R_3(\lambda) + \lambda^3 R_4(\lambda)$, $F_{22} = \lambda^3 R_2(\lambda)$.

From system (5), we obtain the equations for determining the natural frequencies $\lambda = \lambda_i$

$$\Delta = F_{11}(\lambda) \cdot F_{22}(\lambda) - F_{21}(\lambda) \cdot F_{12}(\lambda) = 0. \quad (6)$$

The eigenfunctions of the boundary value problem (2) and (3) for equation (1) will be represented as

$$\varphi_i = F_{22}(\lambda_i) Y_1(\lambda_i \xi) + F_{21}(\lambda_i) Y_2(\lambda_i \xi) + (\beta_1 - \alpha_1 \lambda^4) F_{22}(\lambda) Y_4(\lambda_i \xi)$$

The eigenfunctions $\varphi_i(\xi)$ satisfy the orthogonality condition

$$\int_0^1 \varphi_i(\xi) \varphi_k(\xi) d\xi + \alpha_1 \varphi_i(0) \varphi_k(0) + \alpha_2 \varphi_i(1) \varphi_k(1) = 0 \text{ at } i \neq k. \quad (7)$$

Solving an Inhomogeneous Equation

$$W = \sum_{n=1}^{\infty} \varphi_n(\xi) T_n(t), \tag{8}$$

$$\sum_{i=1}^{\infty} (\ddot{T}_i + \omega_i^2 T_i)\varphi_i(\xi) = P\delta(v_0 t / l - \xi) / m_b l, \tag{9}$$

where $\xi = x / l$, $\omega_i = \frac{\lambda_i^2}{l^2}\sqrt{\frac{EJ}{m_b}}$.

Let us write equation (9) at the points ξ=0 and ξ=1

$$\sum_{i=1}^{\infty} (\ddot{T}_i + \omega_i^2 T_i)\varphi_i(0) = P\delta(v_0 t / l) / m_b l, \tag{10}$$

$$\sum_{i=1}^{\infty} (\ddot{T}_i + \omega_i^2 T_i)\varphi_i(1) = P\delta(v_0 t / l - 1) / m_b l. \tag{11}$$

By multiplying equality (9) by $\varphi_k(\xi)$, $\alpha_1\varphi_k(0)$ and $\alpha_2\varphi_k(1)$, respectively, we obtain the following equality

$$\sum_{k=1}^{\infty}[(\ddot{T}_i + \omega_i^2)\int_0^1 \varphi_i(\xi)\varphi_k(\xi)d\xi + \alpha_1\varphi_i(0)\varphi_k(0) + \alpha_2\varphi_i(1)\varphi_k(1)] = \frac{P}{m_b l}[\varphi_k(v_0 t / l) +$$

$$+ \alpha_1\varphi_k(0)\delta(v_0 t / l) + \alpha_2\varphi_k\delta(v_0 t / l - 1)].$$

Using the orthogonality condition (7), we obtain

$$\ddot{T}_k + \omega_k^2 T_k = F_k[\psi(v_0 t / l) + \alpha_1\varphi_k(0)\delta(v_0 t / l) + \alpha_2\varphi_k(1)\delta(v_0 t / l - 1)]. \tag{12}$$

Here $F_k = \frac{P}{\|\varphi_k\| m_b l}$, $\|\varphi_k\| = \int_0^1 \varphi_k^2(\xi)d\xi + \alpha_1\varphi_k^2(0) + \alpha_2\varphi_k^2(1)$.

$\psi_k(z)=\varphi_k(z)$ for z≤1, φ_k=0 for z≥1.
$\psi_k(z)=\varphi_k(z)$ for z≤1, ψ_k=0 for z≥1.

Given zero initial data, equation (12) has a solution in the following form:

$$T_k = \frac{F_k}{\omega_k}\left\{\int_0^t \psi_k(v_0\tau / l)\sin\omega_k(t-\tau)d\tau + \frac{l}{v_0}[\alpha_1\varphi_k(0)\sin(\omega_k t) + \alpha_2\varphi_k(1)\sin\omega_k(t - l / v_0)]H(t - l / v_0)\right\}$$

$H(z)$ is a Heaviside function.

3 Results and Discussion

Figure 4, a shows plots of the distribution of beam deflections along the length $W(\xi, t)$ (m) for three values of stiffness coefficients of supports $k_1=k_2=k$ of a rectangular section with sides a_0 and b_0 at different moments of time.

The calculations take: l=22 m, m_b=889 kg/m, $m_1=m_2$=2500 kg, $E=5\cdot10^{10}$ MPa, J=0.00312 m^4, v_0=40 km/h, P=200 kN, $S_1=S_2=2(a_0+b_0)$, a_0=0.35 m, b_0=0.35 m. The time of

action of the moving uniform load on the beam is $t_0=l/v_0=1.98$ sec. Fig. 5 shows the deflection plots for the time moment $0<t<2t_0$.

From the graphs of deflection changes W, shown in Fig 4, it follows that for the moment $0<t<t_0$, the greatest deflections occur in the section $x=0.5l$ at a time when the load reaches this and the end sections (curves 2 and 4) of the beam. Maximum deflections are achieved in sections $x=0$ and $x=l$ at the time $t=t_0$. The same pattern of change in beam deflections along the coordinate occurs for time $t_0<t<2t_0$.

The graphs of stress distribution along the beam sections at different moments of time t(s) are shown in Fig. 4, *b*. At time moments $t=0.5t_0\approx1$ sec and $t=t_0\approx2$ sec (curves 2 and 4), maximum stress values 20 MPa with positive and negative signs are reached in sections $x=0.5l$ and $x\approx0.85l$ at time moment $t=0.5t_0$ (the moving load will be in the middle or close to the end section of the beam).

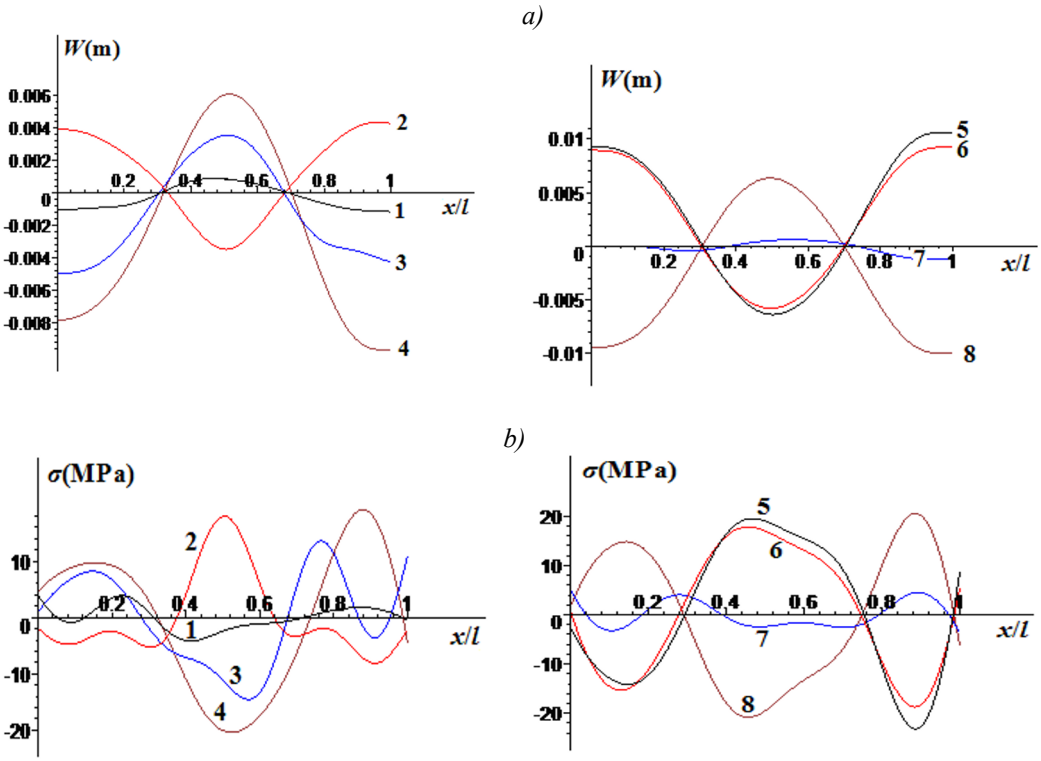

Fig. 4. Distribution of beam deflections W(m) along the length (*a*) and longitudinal stresses σ(MPa) (*b*) for $k=10^5$ N/m^2 and different time moments t(s): 1–$t=0.25t_0$, 2–$t=0.5t_0$, 3–$t=0.75t_0$, 4–$t=t_0$, 5–$t=1.25t_0$, 6 – $t=1.5t_0$, 7–$t=1.75t_0$, 8–$t=2t_0$

The analysis of the results of the calculations performed for the other two stiffness values $k_1=k_2=k$ (Fig. 5 *a*, *b* and Fig. 6 *a*, *b*), indicate the preservation of the above patterns of changes in deflections and longitudinal stresses along the x-axis. An increase in the values of the stiffness coefficients affects the laws of change in deflections and stresses along the length of the beam. At the same time, the highest values of deflections of the beam stresses can be achieved in the beam sections $x=0$, $x=0.5$ at the time moments $t=0.5t_0$, $t=0.75t_0$, $t=t_0$, $t=1.25t_0$, $t=1.5t_0$, and $t=2t_0$.

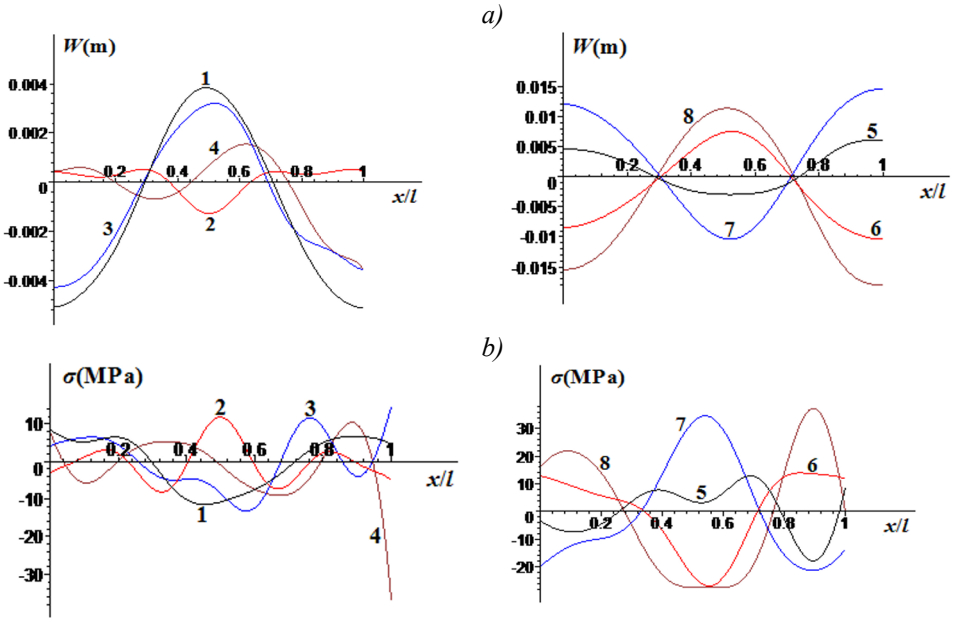

Fig. 5. Distribution of beam deflections W(m) along the length (a) and longitudinal stresses σ(MPa) (b) for k=10^6 N/m^2 and different time moments t(s): 1–t=0.25t_0, 2–t=0.5t_0, 3–t=0.75t_0, 4–t=t_0, 5–t=1.25t_0, 6–t=1.5t_0, 7–t=1.75t_0, 8–t=2t_0

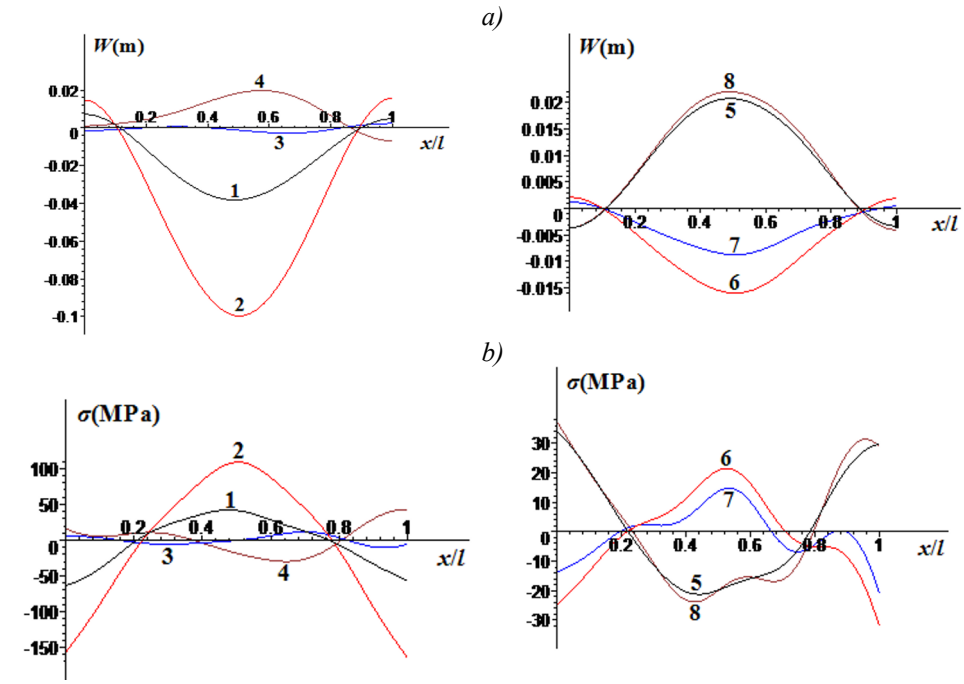

Fig. 6. Distribution of beam deflections W(m) along the length (a) and longitudinal stresses σ(MPa) (b) for k=10^7 N/m^2 and different time moments t(s): 1–t=0.25t_0, 2–t=0.5t_0, 3–t=0.75t_0, 4–t=t_0, 5–t=1.25t_0, 6–t=1.5t_0, 7–t=1.75t_0, 8–t=2t_0

2. Let now the load $P(x, t)$ uniformly distributed on the section of the beam with length L_0 (Fig. 7), determined by the formula ($p_0=P_0/L_0$)
$P=p_0$ for $0<x<v_0t$, $P=0$ for $x>v_0t$, $0<t<L_0/v_0$.
$P=0$ for $0<x<v_0t–L_0$, $P=p_0$ for $v_0t–L_0<x<v_0t$.
$P=0$ for $v_0t<x<l$, $L_0/v_0<t<(l–L_0)v_0$.
$P=0$ for $0<x<v_0t–L_0$, $P=p_0$ for $v_0t–L_0<x<l$, $\frac{l-L_0}{v_0}<t<\frac{l}{v_0}$.
$P=0$ for $0<x<l$, $l/v_0<t<(l+L_0)/v_0$.

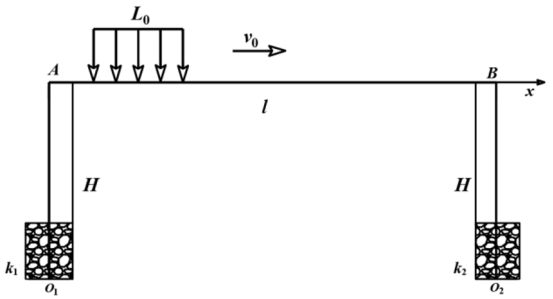

Fig. 7. Calculation scheme of the movable distributed load

Equations (12) for determining the functions $T_k(t)$ in this case have the form

$$\ddot{T}_k + \omega_k^2 T_k = \frac{P_0}{\|\varphi_k\| m_b L_0} F_k(t) \qquad (13)$$

where $F_k = F_{1k} = \int_0^{v_0 t/L_0} \varphi_k(\xi)d\xi + \alpha_1\varphi(0)$ for $0 < t < L_0/v_0$,

$$F_k = F_{2k} = \int_{(v_0t-L_0)/L_0}^{v_0 t/L_0} \varphi_k(\xi)d\xi + \alpha_1\varphi_k(0) \text{ for } L_0/v_0 < t < (l-L_0)/v_0,$$

$$F_k = F_{3k} \int_{(v_0t-L_0)/L_0}^{l} \varphi_k(\xi,k)d\xi + \alpha_1\varphi_k(0) + \alpha_2\varphi_k(1) \text{ for } (l-L_0)/v_0 < t < (l+L_0)/v_0$$

,

$$F_k = F_{4k} = \alpha_1\varphi_k(0) + \alpha_2\varphi(1) \text{ for } t > (l+L_0)/v_0.$$

The solution of equation (13), taking into account the form of the right-hand side, will be represented as

$$T_k = T_{1k} = \frac{A_k}{\omega_k}\int_0^t F_{1k}(\tau)\sin\omega_n(t-\tau)d\tau \text{ for } 0 < t < t_1,$$

$$T_k = T_{2k} = A_k[\frac{1}{\omega_k}\int_{t_1}^t F_{2k}(\tau)\sin\omega_n(t-\tau)d\tau + T_{1k}(t_1)\cos\omega_k(t-t_1) + \dot{T}_{1k}(t_1)\sin\omega_k(t-t_1)/\omega_k],$$

for $t_1 < t < t_2$,

$$T_k = T_{3k} = A_k[\frac{1}{\omega_k}\int_{t_2}^{t} F_{3k}(\tau)\sin\omega_n(t-\tau)d\tau + T_{2k}(t_2)\cos\omega_k(t-t_2) + \dot{T}_{2k}(t_2)\sin\omega_k(t-t_2)/\omega_k],$$

for $t_2 < t < t_3$,

$$T_k = T_{4k} = A_k[\frac{1}{\omega_k}\int_{t_4}^{t} F_{4k}\sin\omega_n(t-\tau)d\tau + T_{3k}(t_3)\cos\omega_k(t-t_3) + \dot{T}_{3k}(t_3)\sin\omega_k(t-t_3)/\omega_k],$$

for $t > t_3$,

where $A_k = P_0/\|\varphi_k\|m_b L_0$, $t_1 = L_0/v_0$, $t_2 = (l-L_0)/v_0$, $t_3 = L/v_0$, $t_4 = (l+L_0)/v_0$.

The deflections of the beam sections and the longitudinal stresses are

$$W = \sum_{k=1}^{\infty}\varphi_k(\xi)T_k(t),\ \sigma = \frac{Eh}{L^2}\sum_{k=1}^{\infty}\varphi_k''(\xi)T_k(t).$$

Fig.8-10 shows the graphs of changes in deflections W(m) (*a*) and longitudinal stresses σ(MPa) (b) along the coordinate for three values of the stiffness coefficient $k=k_1=k_2$ (N/m^2) at different times $t=t_i$ (s). In this case, the total time of the distributed load along the beam will be $t=t_4=(l+L_0)/v_0$. The calculations take L_0=5 м, i=1÷8, $t_5=t_4+t_1$, $t_6=t_4+t_2$, $t_7=t_4+t_3$, $t_8=2t_4$.

Then we have t_1=0.45 sec, t_2=1.53 sec, t_3≈2 sec, t_4=2.43 sec, t_5=2.83 sec, t_6=3.91 sec, t_7=4.17 sec, t_8=4.86 sec.

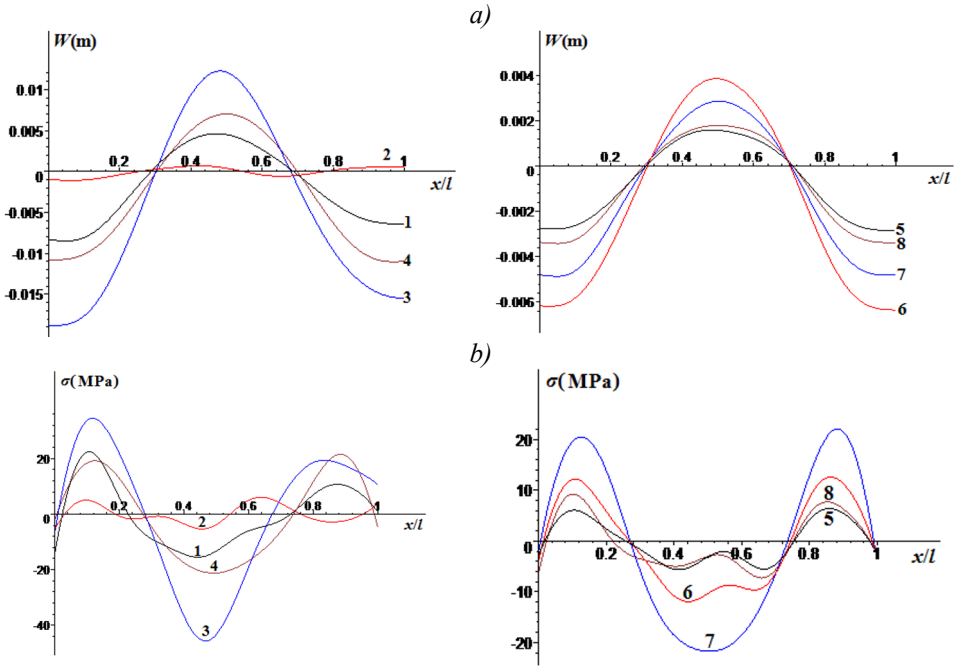

Fig. 8. Distribution of beam deflections W(m) along the length (*a*) and longitudinal stresses σ(MPa) (*b*) for $k=10^5$ N/m^2 and different time moments t(s): 1–$t=t_1$, 2–$t=t_2$, 3–$t=t_3$, 4–$t=t_4$, 5–$t=t_4+t_1$, 6–$t=t_4+t_2$, 7–$t=t_4+t_3$, 8–$t=2t_4$

An analysis of the curves shows that the greatest deflections and stresses occur in the middle section of the beam at the time t=0.45 sec and t=2.83 sec and are periodic in time. An increase in the stiffness coefficient value of the coupling with the ground medium leads to an increase in stresses in the beam sections. This legitimacy is most convincingly noticed at high values of the coefficient k (Fig.10. *b*). The above general regularity under the action of a moving concentrated force also takes place in the case of the action of a uniform distributed load.

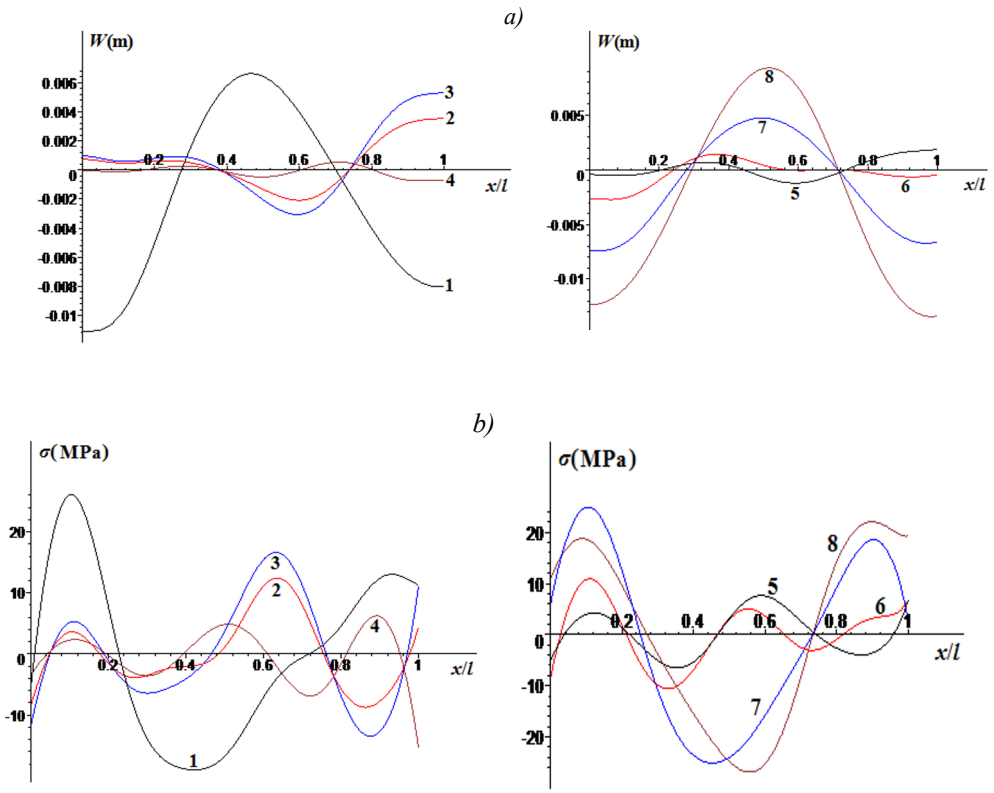

Fig. 9. Distribution of beam deflections W(m) along the length (*a*) and longitudinal stresses σ(MPa) (*b*) for k=10^6 N/m^2 and different time moments t(s):1–t=t_1, 2–t=t_2, 3–t=t_3, 4–t=t_4, 5–t=t_4+t_1, 6–t=t_4+t_2, 7–t=t_4+t_3, 8–t=2t_4

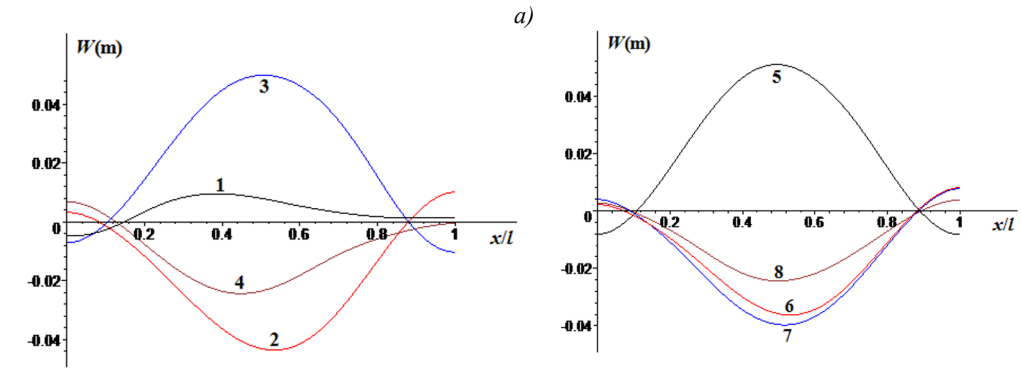

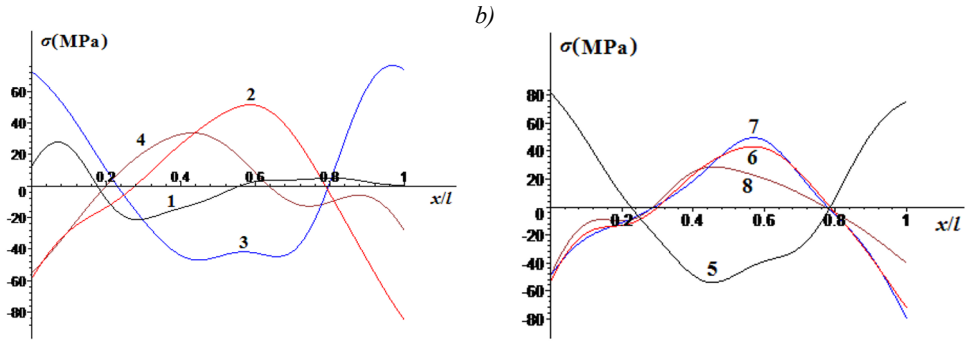

Fig. 10. Distribution of beam deflections W(m) along the length (a) and longitudinal stresses σ(MPa) (b) for k=10^7 N/m^2 and different time moments t(s):1–t=t_1, 2–t=t_2, 3–t=t_3, 4–t=t_4, 5–t=t_4+t_1, 6–t=t_4+t_2, 7–t=t_4+t_3, 8–t=2t_4

4 Conclusion

The action of a moving uniform load on the beam results in the occurrence of maximum longitudinal forces in the initial, middle, and end sections of the beam at the moment when the load passes through those sections.

After completing a moving uniform load, the laws of stress change along the coordinate are practically independent of time.

An increase in the stiffness coefficient of the elastic connection between the supports and the ground has a different effect on the character of the stress change along the x-axis. Thus, at high coefficient values, the laws of voltage change along the coordinate are practically independent of time. In this case, as the value of this coefficient increases, the stress values in the beam sections increase.

When a concentrated load is applied, depending on the stiffness coefficient of the connection between the supports and the ground, stresses exceeding the limit load can occur in the middle of the beam cross-section. Thus, in the calculations, it is necessary to consider the nature of the interaction of the supports with the surrounding soils when calculating the beams for the action of moving loads.

References

1. M. Berdibaev, B. Mardonov, and A. Khurramov, in *E3S Web Conf.* (2021).
2. Y. Khadri, S. Tekili, E. M. Daya, A. Daouadji, M. Guenfoud, and B. Merzoug, Int. Rev. Mech. Eng. (2009).
3. L. Fry'ba and C. R. Steele, J. Appl. Mech. (1976).
4. S. H. Ju, Soil Dyn. Earthq. Eng. (2007).
5. Y. Xiao, X. Luo, J. Liu, and K. Wang, Adv. Civ. Eng. (2020).
6. Y. S. Cheng, F. T. K. Au, and Y. K. Cheung, Eng. Struct. (2001).
7. A. Garinei and G. Risitano, Eng. Struct. (2008).
8. Z. Wang, Y. Shi, X. You, R. Jiang, and W. Gai, Materials (Basel). (2021).
9. X. Li, J. Ren, and X. Liu, in (2018).
10. M. Miralimov, A. Ishankhodjaev, K. Almenov, and E. Muminov, in *E3S Web Conf.* (2021).

11. S. S. Law and X. Q. Zhu, Eng. Struct. (2004).
12. H. C. Kwon, M. C. Kim, and I. W. Lee, Comput. Struct. (1998).
13. J. Li, H. Zhang, D. Zhu, and C. Li, Eur. J. Mech. A/Solids (2022).
14. S. Y. Zhang, X. Sheng, J. Z. Jiang, H. Zhou, W. X. Ren, and Z. H. Zhang, Int. J. Mech. Sci. (2021).
15. P. Lonetti, A. Pascuzzo, and A. Davanzo, Math. Probl. Eng. (2016).
16. J. Senthilvasan, D. P. Thambiratnam, and G. H. Brameld, Eng. Struct. (2002).
17. M. Szafrański, Roads Bridg. - Drog. i Most. (2018).
18. I. Al-abboodi, O. Al-salih, and A. Dakhil, J. King Saud Univ. - Eng. Sci. (2021).
19. X. Q. Zhu and S. S. Law, J. Sound Vib. (2001).
20. C. Bilello and L. A. Bergman, J. Sound Vib. (2004).